Determination of the ^{161}Tb half-life

S.M. Collins [a,b,*], C. Gilligan [c], B. Pierson [d], N. Ramirez [a], M. Goodwin [b,c], A.K. Pearce [a], B. C. Archambault [d], M.M. Haney [d], P.H. Regan [a,b]

[a] National Physical Laboratory, Hampton Road, Teddington, Middlesex, TW11 0LW, United Kingdom
[b] Department of Physics, University of Surrey, Stag Hill, Guildford, GU2 7XH, United Kingdom
[c] Atomic Weapons Establishment, Aldermaston, Reading, Berkshire, RG7 4PR, United Kingdom
[d] Pacific Northwest National Laboratory, 902 Battelle Blvd, Richland, WA, 99354, United States

A B S T R A C T

There is significant interest in the use of terbium radioisotopes for applications in cancer therapy and diagnosis. Of these, ^{161}Tb, as a medium energy beta-emitter, is being investigated as a potential alternative to ^{177}Lu. The relatively high proportion of conversion electron and Auger electron emissions per decay make ^{161}Tb an attractive targeted therapeutic. As a product of nuclear fission, ^{161}Tb is also of importance to nuclear forensics. The standard uncertainty of the current evaluated half-life of 6.89(2) d contributes significantly to the standard uncertainty of any decay corrected activity determination made. Furthermore, the accuracy of this evaluated half-life has been called into question by measurements reported in 2020 at the Institute of Radiation Physics (IRA), Switzerland, who reported a half-life of 6.953(2) d. In the current work, the half-life of the ^{161}Tb ground state decay has been measured at three independent laboratories located in the United Kingdom and the United States of America for a total of six determinations using three independent measurement techniques; gamma-ray spectrometry, ionisation chamber measurement and liquid scintillation counting. The half-life determined for ^{161}Tb of 6.9637(29) d confirms the observed 1% relative increase observed by IRA, though the reported half-lives in this work and at IRA are significantly different (ζ-score = 3.1).

1. Introduction

There is currently significant interest in the use of four terbium radioisotopes ($^{149,\ 152,\ 155,\ 161}$Tb), which have been identified as having suitable physical characteristics (half-life, emission type and gamma-ray intensity) for applications in cancer therapy and diagnosis (Müller et al., 2012). Their matched chemical characteristics make them suitable for attachment to the same targeting vector, allowing them to be coupled and used for unique theragnostic treatment strategies (Müller et al., 2012). Terbium-161, undergoing decay by β^- emission to the ground state of ^{161}Dy with a ground state to ground state endpoint energy of 593.0(13) keV ($E_{\beta av}$ = 154.3 keV), has been posited as a possible alternative for ^{177}Lu for radionuclide therapy (Reich, 2011; Lehenberger et al., 2011; Gracheva et al., 2019). These two radionuclides share similar characteristics as medium-energy beta-particle emitters with low-energy gamma-ray emissions, however ^{161}Tb enjoys a higher proportion of conversion electron emissions, arising from the low-energy transitions (depicted in the decay scheme shown in Fig. 1), and Auger electron emissions per decay (~12 e^-, ~36 keV per decay for ^{161}Tb; ~1 e^-, ~1.0 keV per decay for ^{177}Lu) (Eckerman and Endo, 2008; Müller et al., 2014). These additional low-energy particle emissions provide an advantage in delivering a cytotoxic dose to micro-metastases and single tumour cells whilst sparing surrounding non-tumorous cells when coupled with a targeting agent (Haller et al., 2016; Müller et al., 2012; Ku et al., 2019). It has also been shown that the use of single-photon emission computer tomography (SPECT) imaging is feasible with ^{161}Tb due to the emission of the low-energy gamma-rays, reducing the need for a combined theragnostic treatment approach (Marin et al., 2020).

Before any radiopharmaceutical can be used clinically the administered activity must be determined so that the whole-body dose to the patient can be determined; this is typically performed via a radionuclide calibrator with traceability to a national metrology institute. As discussed in Durán et al. (2020) the magnitude of the standard uncertainty on the recommended half-life for ^{161}Tb of 0.28% does not lend itself well to defining a precise primary standardisation. The half-life is also an important factor for modelling the dose delivered to a patient or tumour or determining the expiration time and specific activity of the treatment. Therefore, it is of particular interest that the half-life be determined with a greater precision.

Whilst the production of ^{161}Tb for medical applications has been developed and optimised through the ^{160}Gd(n,γ)^{161}Gd→^{161}Tb nuclear reaction and decay process (Lehenberger et al., 2011; Gracheva et al., 2019) it can also be produced following nuclear fission at very low

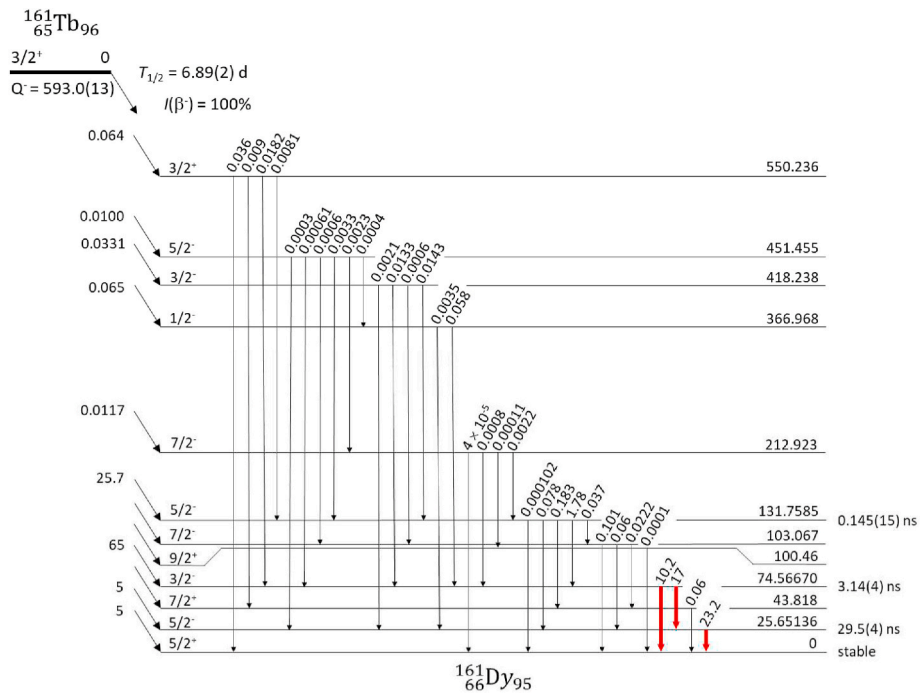

Fig. 1. Decay scheme of ^{161}Tb taken from the evaluation of Reich (2011). The uncertain gamma transitions have been omitted. The major characteristic gamma ray transitions are identified as bold red arrows. (For interpretation of the references to colour in this figure legend, the reader is referred to the Web version of this article.)

Table 1
Measured half-life values from current literature (cut off at December 2020).

Reference	Year	$T_{1/2}$ /d	Method
Butement	1949	6.75(10)	–
Hein and Voigt	1950	7.2(2)	GM counter
Cork et al.	1952	6.8(1)	β spectrometer
Barloutaud and Ballini	1955	7.2(5)	NaI(Tl) spectrometer; β spectrometer
Folgar et al.	1955	6.8	GM counter
Bisi et al.	1956	6.9(1)	β spectrometer
Cork et al.	1956	7.15	β spectrometer
Smith et al.	1956	6.8	Proportional counter
Baranov et al.	1958	7.20(7)	–
Hoffman	1963	6.88(10)	Proportional counter
Funke et al.	1964	7.3(6)	NaI(Tl) spectrometer
Baba et al.	1971	6.90(2)	Proportional counter
Antony and Bueb	1985	6.91(5)	Ge(Li) spectrometer
Abzouzi et al.	1989	6.8985 (4)	Ge(Li) spectrometer
Yongfu et al.	1989	6.954(5)	HPGe spectrometer
Durán et al.	2020	6.953(2)	Ionisation chamber; $CeBr_3$ spectrometry

yields. As a product of nuclear fission, it, along with ^{160}Tb, is an important radionuclide to measure in nuclear forensics samples (Jiang et al., 2017).

At the time of this work, the recommended evaluated ^{161}Tb half-life was 6.89(2) d (Reich, 2011) derived from the weighted average of ten literature values, which have been published between 1949 and 1989 (a number of additional values were also reported with no standard uncertainties). These literature values are presented in Table 1. In Durán et al. (2020), the half-life of ^{161}Tb was measured by three different measurement systems (using two different techniques). Across these three measurement systems a consistently significant increase in the half-life of ^{161}Tb of approximately 1% to the evaluated half-life was observed. Such an increase is at odds with much of the previous literature values and requires verification. In the current paper we report on half-life measurements performed by the National Physical Laboratory (NPL), the Atomic Weapons Establishment (AWE) and Pacific Northwest National Laboratory (PNNL) on the same starting material using four different measurement systems, which confirm the result of the measurement made by Durán et al. (2020).

2. Experimental method

2.1. Production and preparation of ^{161}Tb

The ^{161}Tb was produced at Institut Laue-Langevin, France via the ^{160}Gd(n,γ)^{161}Gd→^{161}Tb nuclear reaction. This was processed by the Paul Scherrer Institute, Switzerland and the resulting 1 g solution of a nominal 100 MBq of $^{161}TbCl_3$ in 0.05 M HCl carrier free was delivered to the NPL.

At NPL, this solution was rinsed from the supplied vial with 4 g of 0.05 M HCl with 10 μg g^{-1} stable Y carrier. A nominal 3 g aliquot (nominal 60 MBq) of the resulting solution was dispensed to a 5 mL ISO ampoule (ISO, 2010) for measurement by the NPL ionisation chamber, a 0.2 g aliquot was diluted with 28 g (solution A) and another 0.6 g aliquot was diluted with 6 g (solution B) of 0.05 M HCl with 10 μg g^{-1} stable Y carrier. From solution B, 1 g aliquots were dispensed to three 2 mL ISO ampoule (ISO, 2010) for analysis by high-purity germanium (HPGe) gamma-ray spectrometry to determine and quantify any radionuclide impurities and to measure the half-life. From solution A, a sample containing 85 kBq of ^{161}Tb in a flame sealed 5 mL BS ampoule (BSI, 1983) was prepared and despatched to the AWE and PNNL.

For the half-life measurements at AWE, 0.1 g aliquots were dispensed to eight 20 mL polyethylene vial each containing 15 mL of Ultima Gold AB liquid scintillation (LS) cocktail (PerkinElmer, Waltham, MA, USA). One additional sample was prepared from a 5 mL aliquot in a 20 mL polyethylene vial for counting by HPGe gamma-ray spectroscopy. Similarly, at PNNL a 0.5 g aliquot of the received solution was dispensed to a polyethylene vial containing 9.5 mL of Ultima Gold AB LS cocktail.

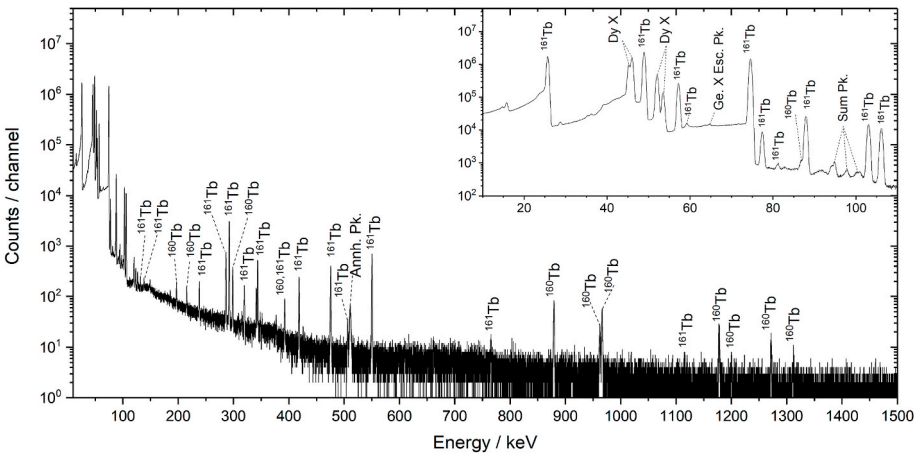

Fig. 2. Gamma-ray spectrum collected with the HPGe gamma-ray spectrometer LOKI. The full-energy peaks of ^{161}Tb and ^{160}Tb are identified. The insert shows the annotated low energy (10 keV–120 keV) region in more detail.

2.2. Ionisation chamber

Ionisation chamber measurements were performed using the NPL secondary standard ionisation chamber system identified as PA782. This system is comprised of two sister TPA MK II ionisation chambers (Sharpe and Wade, 1951, 1953) connected in a 'back-off' formation. The chambers themselves, along with details regarding their lead shielding and connection have been described in detail in previous publications (Fenwick *et al.*, 2016). Each chamber within the system is polarised to voltages of +600 V and – 600 V, with the electrical current produced by each ionisation chamber merging before being fed into an external capacitor. This "back-off" set-up, which employs the use of two chambers set to opposing polarities, has the benefit of reducing the overall background observed by the system. When currents of equal magnitude are detected by both chambers, they effectively cancel each other out, resulting in a net output of zero. This allows for the measurement of lower current sources to be measured to a greater precision. The current of the external capacitor is then read by a Keithley 6430 sub-femtoampere source meter, the measurement frequency of which is governed by an external 4 Hz clock (Stanford Research DG645). In-house software was used to record the observed voltage from the detector system. The stability of the system was monitored through daily background measurements of a ^{226}Ra check source and routine measurement of a set of ^{60}Co check sources of various activities.

2.3. Liquid scintillation counting

At AWE, a 1220 Quantulus LS spectrometer was employed. The instrument employs a built-in dead time correction, with the dead time and linearity of the instrument validated using an ^{90}Y source ($T_{1/2}$ = 2.6684(13) d (Bé et al., 2004)). This validation measurement encompassed the count rate of the ^{161}Tb source (initially 1500 s^{-1}) observed throughout the measurement campaign. Any deviation of the count rate due to dead time and linearity effects was less than 0.1% between 1500 s^{-1} and 30 s^{-1}.

The Quantulus checks the performance of the photomultiplier tubes (PMTs), using a reference LED, and adjusts the high voltage to maintain the signal output. The stability of the instrument was monitored using a ^{14}C check source, with no significant change in the count rate observed throughout the measurement campaign.

The Spectral Quench Parameter of the External Standard (SQP(E)), which refers to the channel below which 99% of the counts of the external standard resides, was determined for each measurement using the instruments external ^{226}Ra source. The quench of the vials was observed to increase over the half-life measurement period of 88 days (a reduction of SQP(E) of less than 0.2 channels per day), this corresponds to a change of less than 0.001% in the calculated counting efficiency per day. The counting efficiency of ^{161}Tb for the measurements collected during for the half-life measurement campaign was modelled to be between 98.9% and 99.0% using the CN2005 software package (Günther, 2002).

Vials containing 0.1 g 0.05 M HCl with 15 mL Ultima Gold AB cocktail were measured before and after each measurement cycle to determine the background count rate, which was on average 0.5 s^{-1} during the measurement campaign.

2.4. High purity Germanium gamma-ray spectrometry

The HPGe gamma-ray spectrometer used by NPL to perform the half-life measurements was a p-type detector (identified as THOR) with a 9.5% relative efficiency and manufacturer specified energy resolution (FWHM) of 581 eV and 1.61 keV at 122 keV and 1.33 MeV respectively. For the radionuclide impurity measurements, a p-type detector (identified as LOKI) with a 22% relative efficiency and energy resolutions of 676 eV and 1.68 keV at 122 keV and 1.33 MeV respectively. Both detectors were contained in Pb shields comprised of 10 cm thick Pb walls covered with 0.5 mm Cd and 0.7 mm Cu graded liner to reduce effects from background radiation and Pb fluorescence X-rays in the spectra. Aluminium optical breadboards were mounted in line with the detector along the horizontal plane with a kinematic mounting plate holding a precision engineered sample holder to provide highly reproducible geometric source positioning. The HPGe gamma-ray spectrometer LOKI and its full-energy peak detection efficiency has been previously detailed in Collins et al. (2019).

The spectra for both detectors were collected using a CANBERRA LYNX digital signal analyser (DSA) connected to a PC running CANBERRA GENIE 2000 v3.4.1. All spectra were collected using the loss-free counting option in the DSA, which had previously been validated to provide correction for dead time and pulse pile-up to within 0.10% over the count rates observed.

At AWE, a Small-Anode Germanium (SAGe) well gamma-ray spectrometer was used for the half-life measurement. The original setup of this system is detailed in Britton and Davies (2015); since then the spectrometer underwent an upgrade to the detector endcap with a (low-Z) thin-window ceramic insert replacing the original window. This improved the absolute full-energy detection efficiency of low-energy photons (~0.61 at 32 keV and ~0.76 at 88 keV). The low-energy resolution (FWHM) for this instrument was reported to be 601 eV and 665 eV at 46.5 keV and 88.0 keV respectively.

The spectra from all HPGe detectors used at AWE were collected using the Canberra LYNX DSA, connected to a Canberra APEX server where the data was archived. The spectra were analysed using a custom

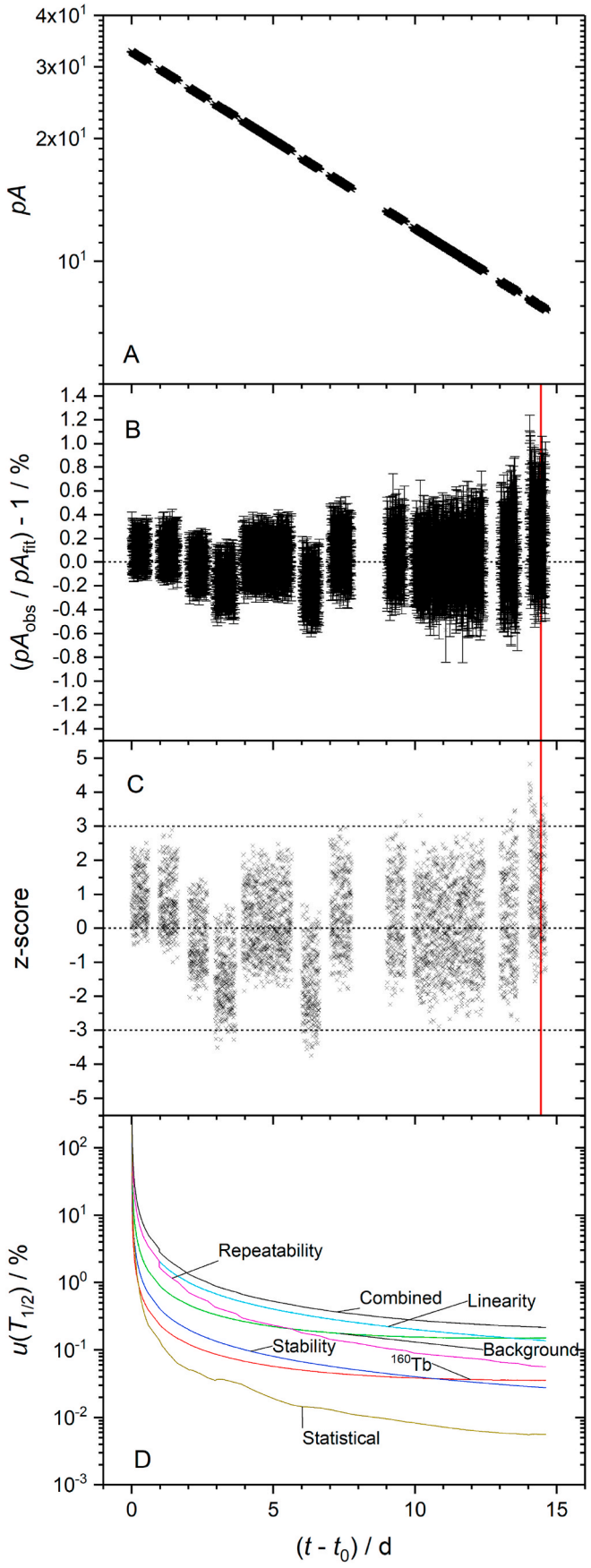

(caption on next column)

Fig. 3. The observed decay of the ^{161}Tb using thePA782 IC at NPL (A), the relative residuals of the least-squares fit (B), the z-scores of the observed data points to the least-squares fit (C) and the uncertainty propagation of the half-life measurement by the NPL ionisation chamber (D). The red line in (B) and (C) indicate where the cut off was applied. (For interpretation of the references to colour in this figure legend, the reader is referred to the Web version of this article.)

ROOT (Brun & Rademakers, 1997) peak-fitting tool. The fitting utility was applied to the data using Python and PyROOT to fit an exponential regression to the corrected net peak areas.

The 20 mL polyethylene vial prepared by AWE (described in section 2.1) was placed inside the detector well with a 3D printed plastic sleeve ensuring a highly reproducible geometric source positioning. This reproducibility of positioning was confirmed experimentally using repeated measurements of a single mixed gamma-ray emitting source. The source was measured a total of twenty times for 3600 s, both with and without repositioning; the standard uncertainty of the sample position repeatability was determined to be less than 0.1 % for 46.5 keV–1173 keV.

A mixed radionuclide quality-check source was also measured every seven days to ensure the detector efficiency was consistent over the data collection period. The count-rate deviation in the 59.5 keV ^{241}Am peak was <0.65 % in all quality-check measurements.

2.5. *Beta-gamma counting system*

At PNNL, the gamma-alpha-beta-gamma (gabγ) coincidence counter was used. This detector system consists of a two photo-multiplier tube (PMT) LS counter and a coincident set of HPGe spectrometers. The PMTs were located on either side of the polyethylene LS vial and sandwiched between two coaxial high-purity gamma-ray spectrometers. The resolution of the two detectors at low energies were measured to have FWHM estimates of 1.2 keV and 1.6 keV at 59.5 keV and 2.2 keV and 2.4 keV at 1332 keV respectively. The lower resolution of these older HPGe detectors reduced the fitting consistency of the low-energy gamma-ray emissions from ^{161}Tb and is reflected in the Compton continuum uncertainty. Data were acquired in list-mode using a CAEN DT5730 digitiser with pulse shape discrimination firmware and a CAEN DT5781 using pulse height analysis for the LS counters and HPGe detectors respectively. These were time-synchronised using a CAEN DT4700 external clock. This allowed for the measurement of the half-life individually by gamma-ray and beta-emission counting components of the system, with self-consistent tracking of the liquid scintillation cocktail response using beta-gamma coincidence counting.

3. Results and uncertainties

3.1. *Radionuclide impurities*

Two of the gamma-ray spectrometry sources prepared at NPL (see section 2.1.) were measured on the HPGe gamma-ray spectrometer LOKI. These were mounted 295 mm from the detector window such that the impact of true coincidence summing on the major peak areas was negligible. The samples were measured for a period greater than 60 000 s.

Terbium-160 ($T_{1/2}$ = 72.3(2) d (Reich, 2005)) was identified in the spectrum (Fig. 2) and its activity determined by the weighted mean of the 879.4 keV, 962.3 keV, 966.2 keV, 1178.0 keV and 1271.9 keV gamma rays, accounting for covariances. The absolute gamma-ray emission intensities were derived from the evaluation of Reich (2005). The resulting activity of ^{160}Tb was 113.7(28) Bq g^{-1} at the reference time of 2019-10-01 12:00 UTC. The activity of the ^{161}Tb was determined through gamma-ray spectrometry using the 57.2 keV and 74.6 keV gamma rays and the nuclear decay data taken from the evaluations of Reich (2011). An activity ratio (A_{Tb160}/A_{Tb161}) at the reference time of

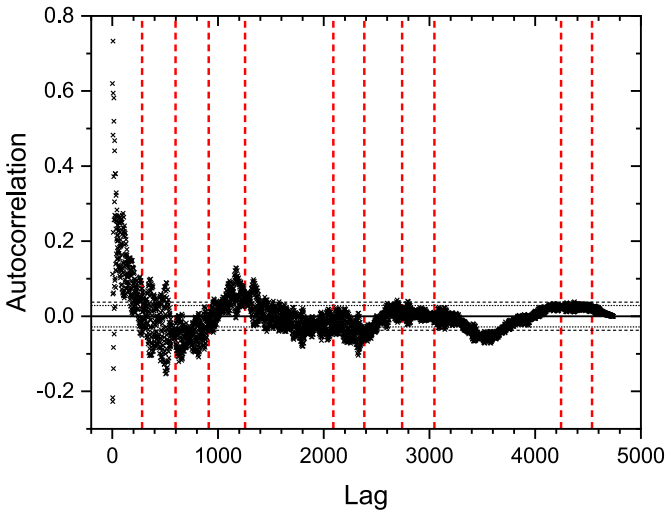

Fig. 4. Autocorrelation factor (ACF) plot for the NPL ionisation chamber. The dashed red lines indicate the points where the sample was repositioned. The dotted and dashed horizontal lines indicate the ACF significance levels at 95% and 99%. The ACF for the varying time lags indicates significant non-randomness (or self-correlation) in the data across the time series. Whilst not perfectly aligned, the times of repositioning and the changes in the ACF trends provide a reasonable indication that the sample repositioning is responsible for the time series trends in the ACF. (For interpretation of the references to colour in this figure legend, the reader is referred to the Web version of this article.)

Table 2
Uncertainty budget for the half-life determined by the PA782 Ionisation Chamber at NPL.

Component	$u(A)$ /%	n	Propagation Factor	$u(T_{1/2})$ /%
Standard deviation of the mean	0.20	4739	0.029	0.0056
Positioning repeatability	0.10	5	0.80	0.080
Stability	0.020	1	1.39	0.028
Linearity	0.10	1	1.39	0.14
^{160}Tb Impurity	0.026	1	1.39	0.036
Background	0.11	1	1.39	0.15
Combined standard uncertainty				0.22

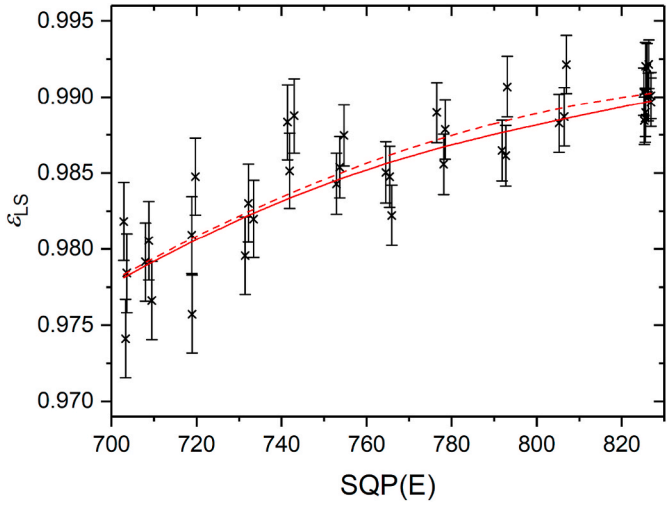

Fig. 5. The calculated LS efficiency (ε_{LS}) curve for ^{161}Tb. The solid and dashed lines represent the modelled LS efficiency curve and experimental LS efficiency curve respectively.

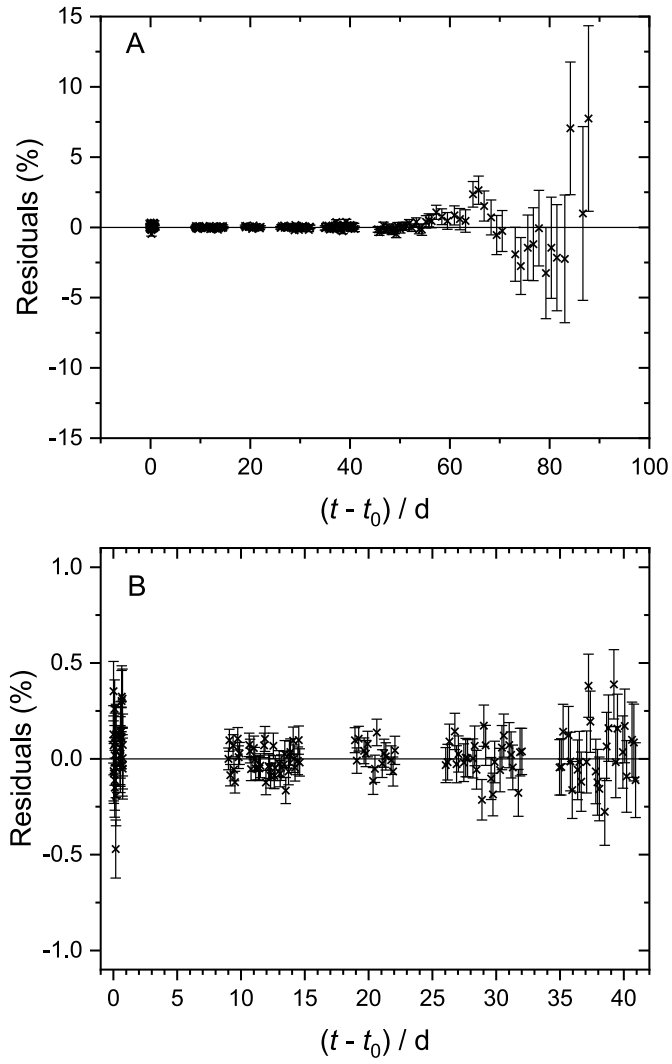

Fig. 6. Residuals for the least-squares fit to the LS corrected count rates at AWE for the (A) full dataset over 88 days and (B) dataset over 41 days used to determine the half-life of ^{161}Tb.

Table 3
Uncertainty budget for the half-life determined by liquid scintillation counting at AWE.

Component	$u(A)$/A /%	n	Propagation factor	$u(T_{1/2})/T_{1/2}$ /%
Standard deviation of residuals	0.040	141	0.06	0.003
Linearity/deadtime	0.10	1	0.49	0.049
Stability	0.10	1	0.49	0.049
Background	0.030	1	0.49	0.015
Quench correction	0.020	1	0.49	0.010
Impurity	0.020	1	0.49	0.010
Combined standard uncertainty			0.072	

0.0001261(38) was determined. The activity of the ^{160}Tb impurity was confirmed by AWE, with an activity ratio at the reference time of 0.0001219(71).

3.2. *Half-life uncertainty evaluation*

The evaluation of the uncertainty components and their propagation

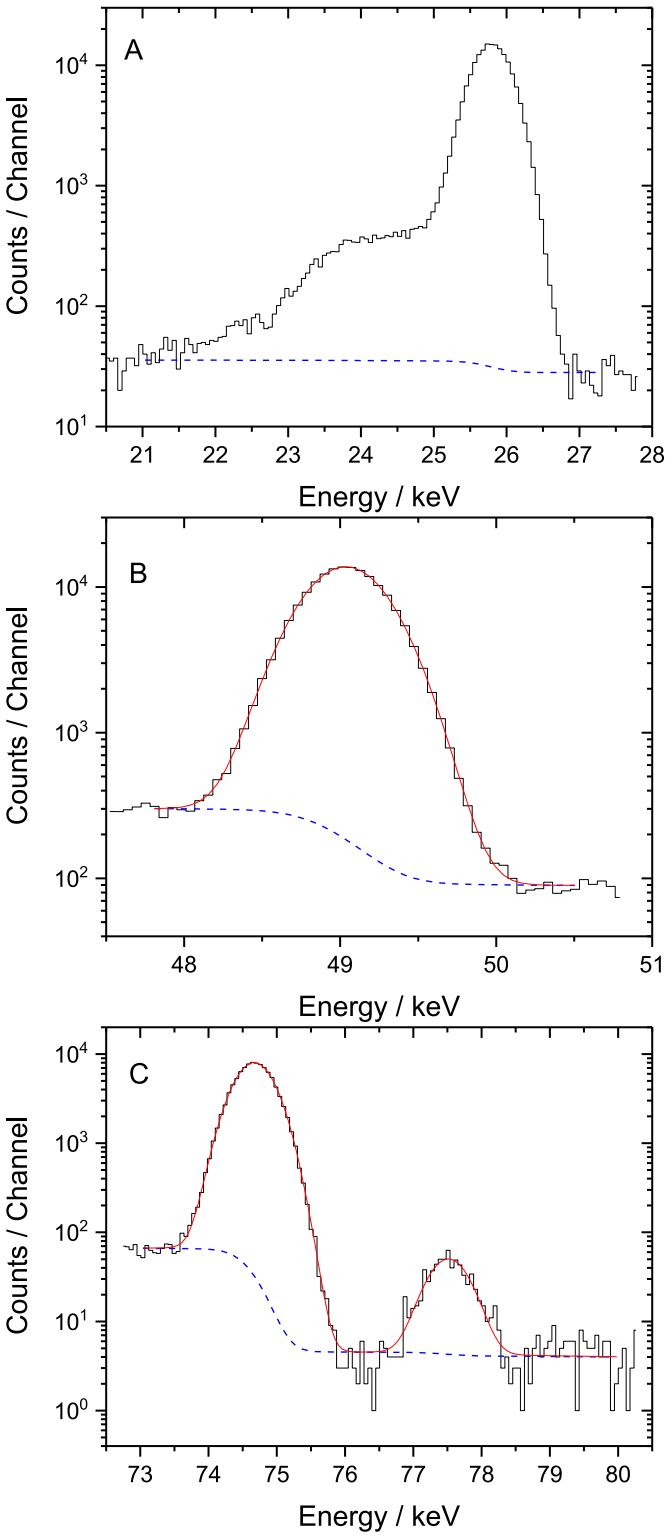

Fig. 7. Examples of full-energy peak fits for the 25.7 keV, 48.9 keV and 74.6 keV gamma rays.

was performed following the recommendations in Pommé (2015). These uncertainty components are typically divided into high-, medium- and low-frequency components, determined by their observed periodicity in the residuals. The calculation of the propagation factors, provided in the uncertainty budget tables later in this paper, were performed using:

$$\frac{\sigma(T_{1/2})}{T_{1/2}} \approx \frac{2}{\lambda t}\sqrt{\frac{2}{n+1}}\,\frac{\sigma(A)}{A} \tag{1}$$

where n is the frequency of instances of the uncertainty component, either the number of measurements (high-frequency) or periodic cycles (medium-frequency) in the data, t is the duration of the measurement campaign, λ is the decay constant, and $\sigma(A)/A$ is the relative uncertainty of the activity from the considered component. By their nature, any periodic nature of low-frequency components is unlikely to be observed and as such $n = 1$ for these components.

3.3. Ionisation chamber

The ionisation chamber (IC) measurements commenced on the 2019-10-01 UTC and were performed over a campaign period of 14.6 d. Due to the number of current measurements performed by the ammeter, with one measurement every 0.25 s, the *pA* measurements within each 180 s acquisition time period were compiled into a single data point (721 measurements) with decay corrections for each 0.25 s measurement to the start of the compiled data point. This produced a dataset containing 4821 data points. Each compiled datapoint was corrected for background and ^{160}Tb response.

The ^{160}Tb response was determined using a calibration factor (CF) that was previously derived from a primary standardisation performed at the NPL. Due to the high energy gamma-ray emissions from the decay of ^{160}Tb the response in the IC is significantly higher than that from the (modelled) ^{161}Tb response, where $CF_{160}/CF_{161} = 24.7(20)$. The background was determined from the average of all background measurements taken over the measurement campaign period, providing a background of - 0.009(14) *pA*. Due to the initial response of the IC to the source (and the magnitude of the uncertainty on the background current) the background correction becomes an increasingly significant source of uncertainty to the half-life measurement as the campaign proceeds (see Fig. 3d). Propagating the background uncertainty component gave an uncertainty of 0.042% and 0.18% on the first and last data point respectively, from an IC response of 32.74 *pA* and 7.74 *pA* respectively.

The sample was removed and replaced in the IC on a total of ten occasions over the course of the measurement campaign. These events can be observed as step changes in Fig. 3b–c. Trends in the dataset were investigated using Autocorrelation analysis, which indicates if elements of a time series are positively or negatively correlated or are independent of each other at varying time lags. In the autocorrelation factor (ACF) plot (Fig. 4), significant trends are apparent within the time-series which when overlaid with the time of the sample repositioning are roughly aligned. It is reasonable to suggest that much of the non-randomness observed in the ACF is because of these sample movements. This geometrical repositioning uncertainty for the activity has been estimated as 0.10% from previous investigations. These source repositioning's are not equidistant as a requirement of Eq. (1). However, in Pommé and De Hauwere (2020) this effect on the uncertainty estimation is discussed and identified that this uncertainty propagation still provides a relatively robust estimator. The distribution of time intervals can, however, lead to overestimations or underestimations in the uncertainty. The sample was repositioned ten times but due to the time intervals being weight to the start and middle of the campaign a decision was made to reduce this to $n = 5$ for the purposes of the uncertainty propagation.

The half-life was determined using a weighted least-squares fit to the background and impurity corrected data points using the expression:

$$I(t) = I(0).e^{-\lambda t} \tag{2}$$

where I is the current, t is the time elapsed since the start of the first measurement and λ is the decay constant of ^{161}Tb. No correction was

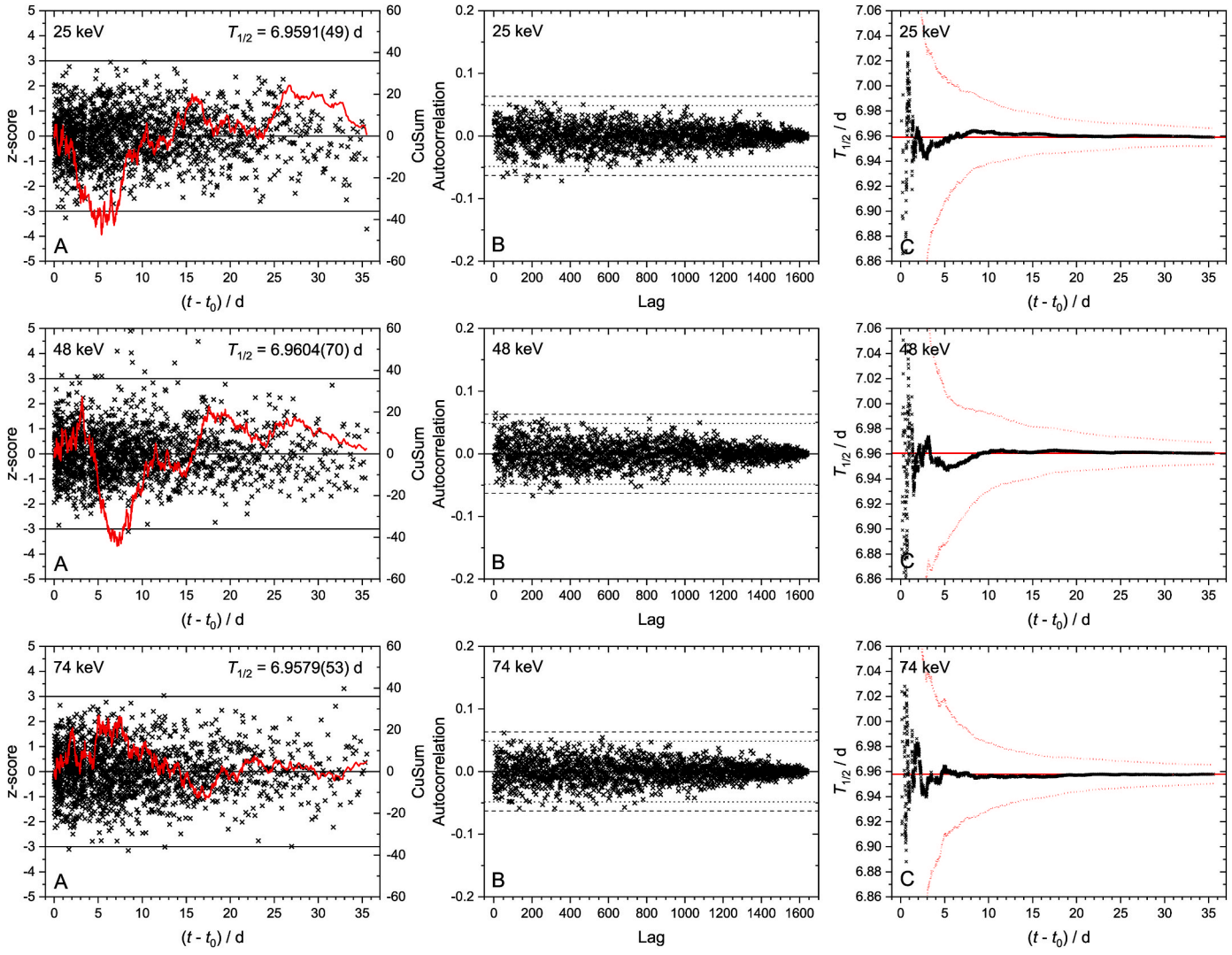

Fig. 8. Residuals (A), as z-scores, of the least-squares fit to the 25.7 keV, 48.9 keV and 74.6 keV gamma-ray datasets at NPL. The cumulative summation (CuSum) of the z-scores are shown on each residuals plot. The half-lives determined for each dataset is shown on the plot for each energy. The quoted combined standard uncertainty is comprised of only the independent components of each dataset (the standard deviation of the residuals, trends in the residuals and peak fitting). The (B) autocorrelation factor (ACF) plots for each energy dataset indicate that there were no significant cyclical periods in the data. The ACF can be seen to be within the 95% and 99% significance levels (dotted and dashed lines respectively) for the majority of time-lag separations and no significant trends present indicting that the data is random. The (C) 'forward' evolution of the half-life indicates that stability in the measured half-life is achieved after approximately 8 days in the three datasets. The half-life determined for the dataset is shown by the solid red line and the evolution of the standard uncertainty by the dotted red line. (For interpretation of the references to colour in this figure legend, the reader is referred to the Web version of this article.)

Table 4
Uncertainty budget for the half-life determined by the HPGe gamma-ray spectrometer at NPL. The half-life result is the weighted mean of the three results for the different gamma rays used.

Component	25.7 keV				48.9 keV				74.6 keV			
	$u(A)$ /%	n	Propagation factor	$u(T_{1/2})$ /%	$u(A)$ /%	n	Propagation factor	$u(T_{1/2})$ /%	$u(A)$ /%	n	Propagation factor	$u(T_{1/2})$ /%
Standard deviation of residuals	0.25	1640	0.020	0.0050	0.30	1640	0.020	0.0058	0.34	1640	0.020	0.0067
Trends in residuals	–	–	–	0.032	–	–	–	0.029	–	–	–	0.019
Peak/continuum fitting	0.11	1	0.565	0.062	0.17	1	0.565	0.096	0.13	1	0.565	0.073
Results/energy	6.9591(49)			0.070	6.9604(70)			0.10	6.9579(53)			0.076
Peak/continuum fitting	0.10	1	0.565	0.057								
Efficiency stability	0.10	1	0.565	0.057								
Dead time/pulse pile-up	0.10	1	0.565	0.057								
$T_{1/2}$	6.9589(64)			0.093								

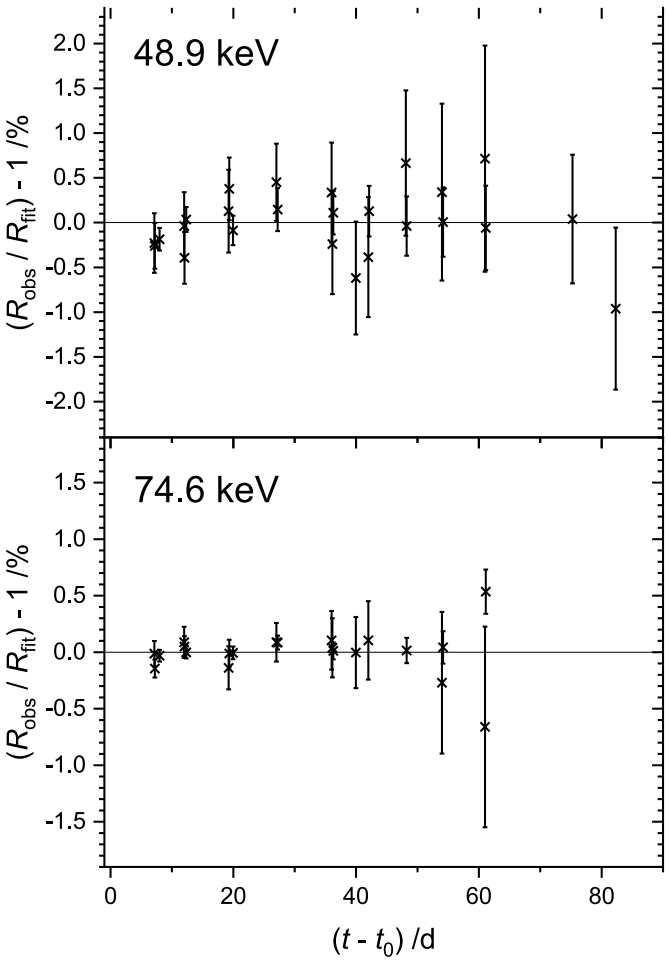

Fig. 9. Residuals of the least-squares fit to the 48.9 keV and 74.6 keV of the AWE datasets.

made for decay during the measurement period (180 s) as this has been applied during the compilation process. With each new iteration of the determined half-life the compilation process was repeated until the there was no change in the half-life determined. As the length of the compiled measurements were short compared to the half-life, this affect was negligible and only required a single iteration. The weight of each data point was determined using the combined uncertainty of the standard deviation of the mean of the 721 measurements, the geometrical repeatability uncertainty, the propagated background uncertainty and the propagated ^{160}Tb impurity correction uncertainty.

The uncertainty budget is given in Table 2. As the half-life propagation of the uncertainty components for the background and ^{160}Tb impurity correction has an increasing influence on the precision of the half-life measurement as the campaign continued, there becomes a point where the inclusion of further data points does not lead to further precision and can actually adversely lead to a decrease in the precision. Through the analysis of the propagated uncertainty components over the duration of the campaign it was identified that no further improvement in the precision was achievable after 14.45 d. This time is indicated in Fig. 3b-c. The half-life was therefore determined using 4739 data points from the total 4821 data points. The half-life determined via the IC was 6.964(15) d.

3.4. *Liquid scintillation counting*

At AWE, the measurement campaign commenced on 2019-10-16 and continued over a period of 88 days. A total of 189 measurements were performed with increasing acquisition times, ranging from 300 s to 96 000 s. Each measurement was corrected for the background, the presence of the ^{160}Tb and for the decay during measurement.

To determine the impact of the ^{160}Tb contribution to the observed count rate the CIEMAT-NIST efficiency tracing technique was applied to determine the LS counting efficiencies of the ^{161}Tb and ^{160}Tb (Grau and Garcia-Toraño, 1982). The determination of the LS counting efficiencies for ^{161}Tb have previously been detailed in Jiang et al. (2015). A series of vials were prepared with a ^{3}H standard traceable to national standards and measured with increasing quantities of nitromethane to test the modelled counting efficiency. In Fig. 5 the LS efficiency tracing curve for ^{161}Tb is shown, with the least-squared fit of the observed data and the modelled curve showing a similar trend. The calculated LS counting efficiencies for ^{161}Tb and ^{160}Tb were 0.9888–0.9897 and 0.9930–0.9937 respectively. These were used to correct the ^{161}Tb count rate for the ^{160}Tb contaminant.

The half-life was determined using a least-squares fit to the observed ^{161}Tb count rates. The count rates were again corrected for decay during measurement and the process repeated iteratively to find the minimum R^2 value. The residuals of the least-squares fit are shown in Fig. 6. The standard uncertainty of the ^{161}Tb half-life measured by liquid scintillation counting reached a minimum for the data set collected up to $(t\text{-}t_0) =$ 41 d ($n = 141$). For measurements after this period the uncertainty increases as relative corrections for the background and longer lived ^{160}Tb impurity became more significant. The half-life of ^{161}Tb determined via liquid scintillation counting at AWE was 6.9619(50) d. The uncertainty budget is shown in Table 3.

Table 5
Uncertainty budget for the half-life determined by the HPGe gamma-ray spectrometer at AWE. The half-life result is the weighted mean of the two results for the different gamma rays used.

Component	48.9 keV				74.6 keV			
	$u(A)$ /%	N	Propagation factor	$u(T_{1/2})$ /%	$u(A)$ /%	N	Propagation factor	$u(T_{1/2})$ /%
Standard deviation of residuals	0.38	27	0.066	0.025	0.09	21	0.074	0.0067
Trends in residuals	–	–	–		–	–	–	
Results/energy	6.9661(18)			0.025	6.9665(4)			0.0067
Peak/continuum	0.65	1	0.248	0.057				
Fitting								
Reproducibility								
Efficiency stability								
Dead time/pulse pile-up	0.10	1	0.248	0.057				
$T_{1/2}$	6.9664(59)			0.085				

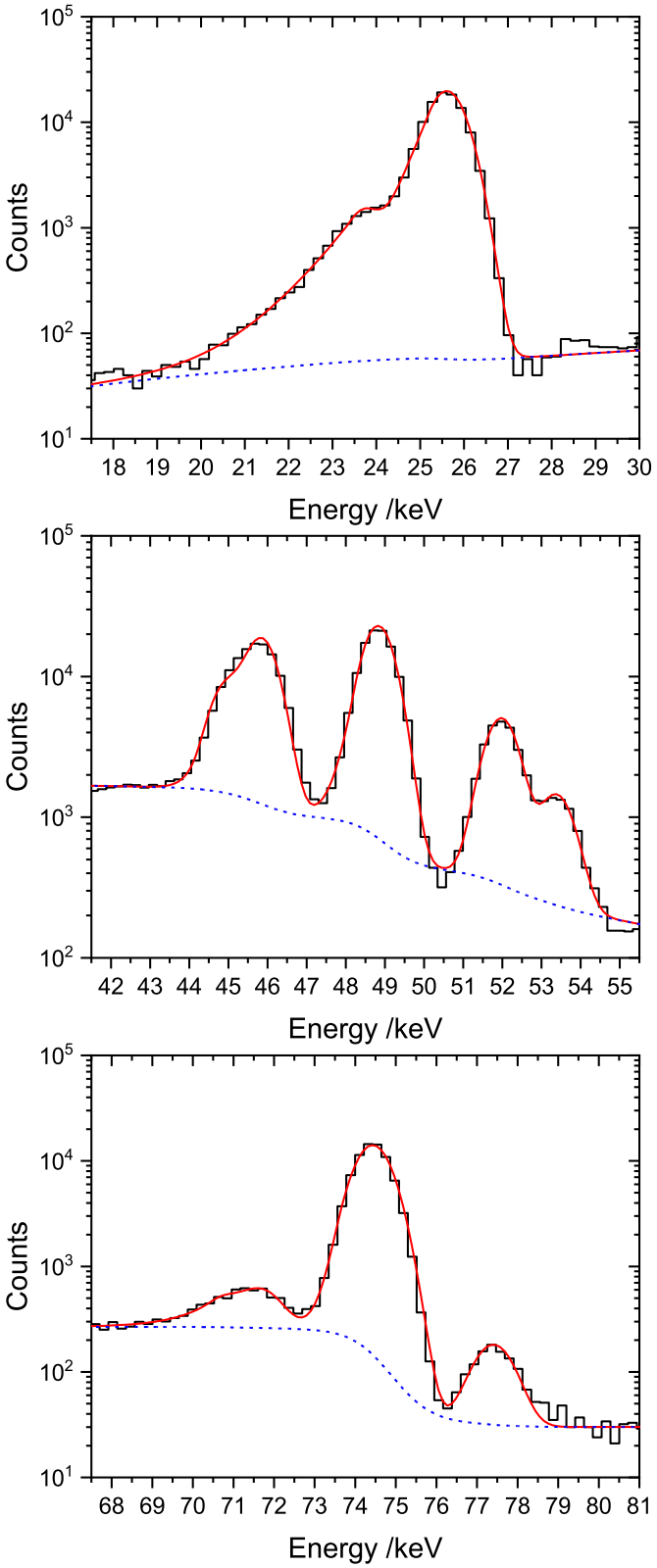

Fig. 10. Illustrations of fits to the 25.7 keV, 48.9 keV, and 74.6 keV regions by PNNL. The initial seed guess for the fit, the final fit, and the continuum are provided for reference.

3.5. HPGe gamma-ray spectrometry

At NPL, the measurement campaign commenced on the 2019-10-09 UTC and proceeded to collect 1640 spectra over a period of 35.6 d (approximately 5.1 half-lives). These measurements were performed such that 100 000 counts were collected in the 74 keV net peak area before commencing the next measurement. This resulted in the live time of the measurements at $t = 0$ of approximately 465 s and at $t = 35.6$ d of approximately 16 140 s.

The 25.7 keV, 48.9 keV and 74.6 keV peak in each spectrum were fitted using an internally developed Microsoft Excel based software package (Fig. 7) (Collins et al., 2020). As a result of significant Compton scattering within the sample the full-energy peak of the 25.7 keV gamma-ray is a challenge to fit as it is a superposition of the full-energy peak and the Compton scattered gamma rays emanating from the source and intervening materials. Therefore, to achieve a consistent fit the net area was taken as the sum of the full-energy peak and the Compton scattering component above the Continuum (Fig. 7a). For the 48.9 keV and 74.6 keV full-energy peaks a Gaussian function with additional low-energy and high-energy tail components were used (Collins et al., 2020). Unlike for the AWE measurements, described later, the Pb X-rays from the surrounding shield did not interfere with the peak fitting of the 74.6 keV full-energy peak. This is explained through the difference in activity of the two samples used by NPL and AWE and the geometry and size of the detector crystal in regard to the Pb shield, where the NPL detector is significantly smaller and the Pb-Detector distance is much greater.

The half-life was determined for each dataset for a specific gamma-ray energy using a weighted non-linear least-squares fit to the observed count rates, accounting for decay to the end of the measurement, using:

$$R(t) = R(0).e^{-\lambda t}.\frac{1 - e^{-\Delta t\lambda}}{\Delta t\lambda} \tag{3}$$

where Δt is the live time.

The residuals, as z-scores ($(x_{obs} - x_{exp})/\sigma_{obs}$ (ISO, 2015)), for each least-squares fit are shown in Fig. 8. The residuals for the gamma-ray datasets were investigated for trends using the cumulative summation (CuSum) of the z-score and through autocorrelation analysis (ISO, 2011; Collins et al., 2015a; Collins et al., 2015b). The autocorrelation analysis (Fig. 8b) showed no observable periodic oscillations in the residuals. However, the CuSum analysis (Fig. 8a) showed some possible 'hidden structure' within the first seven days. Through sampling of different start points of the datasets (e.g. $(t - t_0) = 5$ d), the effect of the CuSum 'structure' on the half-life was estimated and an additional uncertainty component included to account for the effects of these on the measured half-life (Table 4).

As mentioned earlier, the fit of the 25.7 keV region was performed with a different approach (Fig. 7a). However, the uncertainty budget for each gamma-ray emission showed a more precise of the three for the 25.7 keV dataset (Table 4). This was primarily from the estimation of the uncertainty from the 'peak' area fitting and continuum subtraction. This component was estimated by varying the region of interest (ROI) around the full-energy peaks and deriving an uncertainty from the range of half-lives determined. For the 25.7 keV the continuum subtraction of the ROI was relatively flat, whilst the 48.9 keV and 74.6 keV full-energy peak regions where not as smooth. For example, the 48.9 keV full-energy peak sits between the K_α (45.2–46.0 keV) and K_β (48.9–52.2 keV) ^{161}Dy x-ray peak regions (see insert in Fig. 1) and so sits upon their high and low energy tails respectively. The continuum subtraction for the 74.6 keV full-energy peak is complicated by the presence of the 77.4 keV full-energy peak.

The half-lives determined for each gamma-ray dataset were consistent within the combined uncertainty of the standard deviation of the residuals, the trends and peak fitting components. The final half-life of

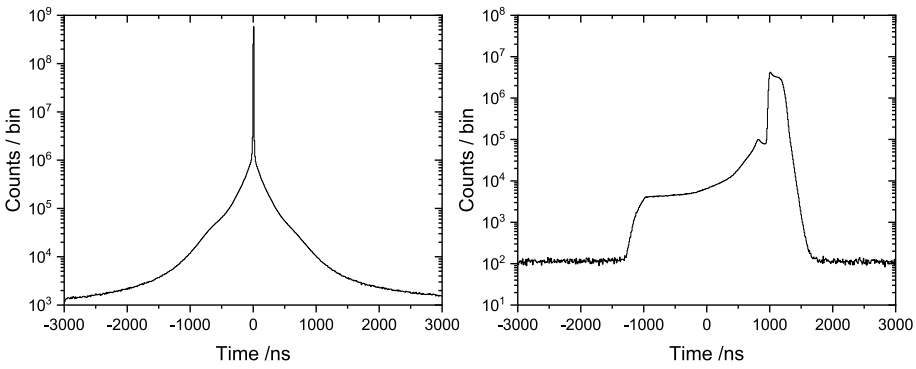

Fig. 11. Time-difference histograms between the two PMTs (left) and the HPGe and PMT pair (right).

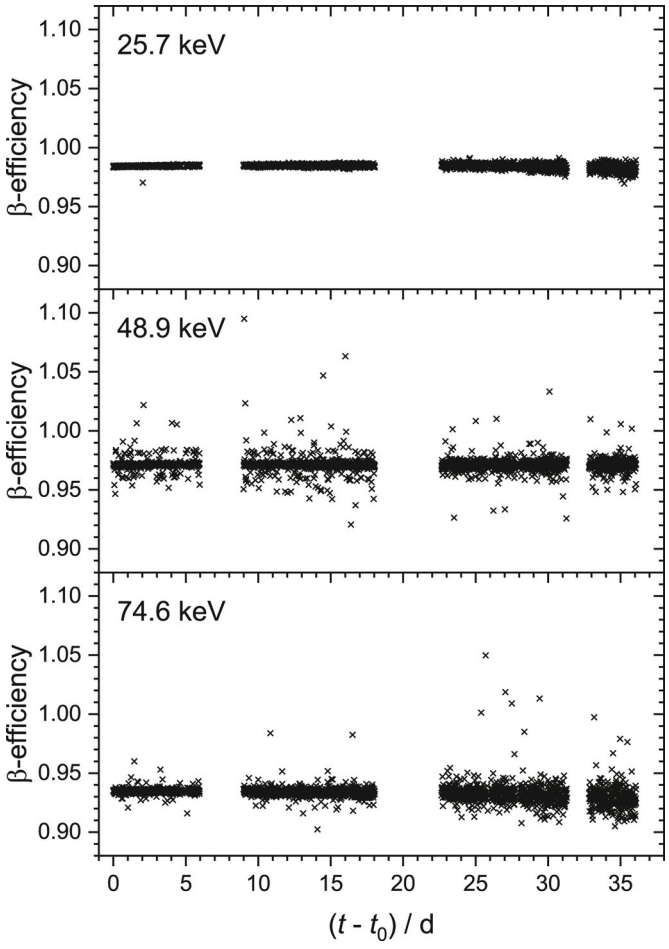

Fig. 12. PNNL LSC beta detection efficiency as a function of time for selected gamma-ray emissions.

Table 6
Uncertainty budget for the half-life determined by liquid scintillation counting at PNNL.

Component	$u(T_{1/2})/T_{1/2}$ /%
Standard deviation of residuals	0.0021
Linearity/deadtime	0.028
Stability	0.00050
Background	0.0077
^{160}Tb Impurity	0.086
Combined standard uncertainty	0.091

the results of each dataset were combined as a weighted mean with the weights of each gamma-ray dataset determined by the combined standard uncertainty of their independent uncertainty components (statistical, residual trends and peak fitting). The final quoted standard uncertainty of the half-life was formed by the inclusion of the correlated uncertainty components (stability, dead time and pulse-pile-up). The full uncertainty is presented in Table 4. The half-life determined by the HPGe gamma-ray spectrometer at NPL was 6.9588(69) d.

At AWE, the measurement campaign commenced on the 2019-10-23 UTC and proceeded to collect 27 spectra over a period of 81 d (~ 11.6 half-lives). These measurements were performed with varying acquisition-times, ranging 3600 s to 250 000 s. The weighted least-squares fit to the datasets for the 48 keV and 74 keV were performed using Eq. (3). No trend was observed between the length of the acquisition and the residuals (Fig. 9). Results from the measurement of the 25.7 keV gamma-ray emission have been rejected, due to the same spectral feature observed in the analysis by the NPL.

The half-lives determined from the 48.9 keV and 74.6 keV gamma-ray emission datasets are in statistical agreement (z-score = 1.0). Later measurements of the 74.6 keV line were rejected due to the impact of Pb fluorescence X-ray interference from the detector cave. The final quoted uncertainty of the half-life includes uncertainty associated with the fitted exponent for each energy, as well as the components of uncertainty associated with peak fitting, reproducibility, efficiency stability and dead time. The full uncertainty is presented in Table 5. The half-life determined by the HPGe gamma-ray spectrometer at AWE was 6.9664 (59) d.

3.6. *Beta-gamma counting with gabγ*

The net peak area of the 25.7 keV, 48.9 keV, and 74.6 keV full-energy peaks were estimated using a multiplet of low-tail gaussians and step functions for each peak and a linear background (Fig. 10). The step height was a scalar fraction of the peak height and was kept the same for all peaks in the multiplet. Segments of data spanning 6000 s were successively isolated from the raw data and fit. The peak area and peak uncertainty were corrected for dead-time, background, and sample mass. The corrected data were fit using Eq. (3).

This same process was repeated but only with gamma-ray transitions that were observed in close time proximity to a beta event. Fig. 11 depicts a set of binned time differences spanning 3 μs on either side of zero for the two PMTs located between the HPGe detectors.

Over 96% of all coincident beta events reside in the time difference window spanning -25 ns–25 ns. The initial sharp decline surrounding the main peak is believed to be rare coincidence assignments between the main beta emission and follow-on conversion electron, predominantly from delayed emission from the 25.7 keV level with a 29.5 ns lifetime. The broader gaussian feature spanning several μs contains rare single coincident events with after pulsing or ringing.

The time-difference plot between the HPGe and PMTs has a different

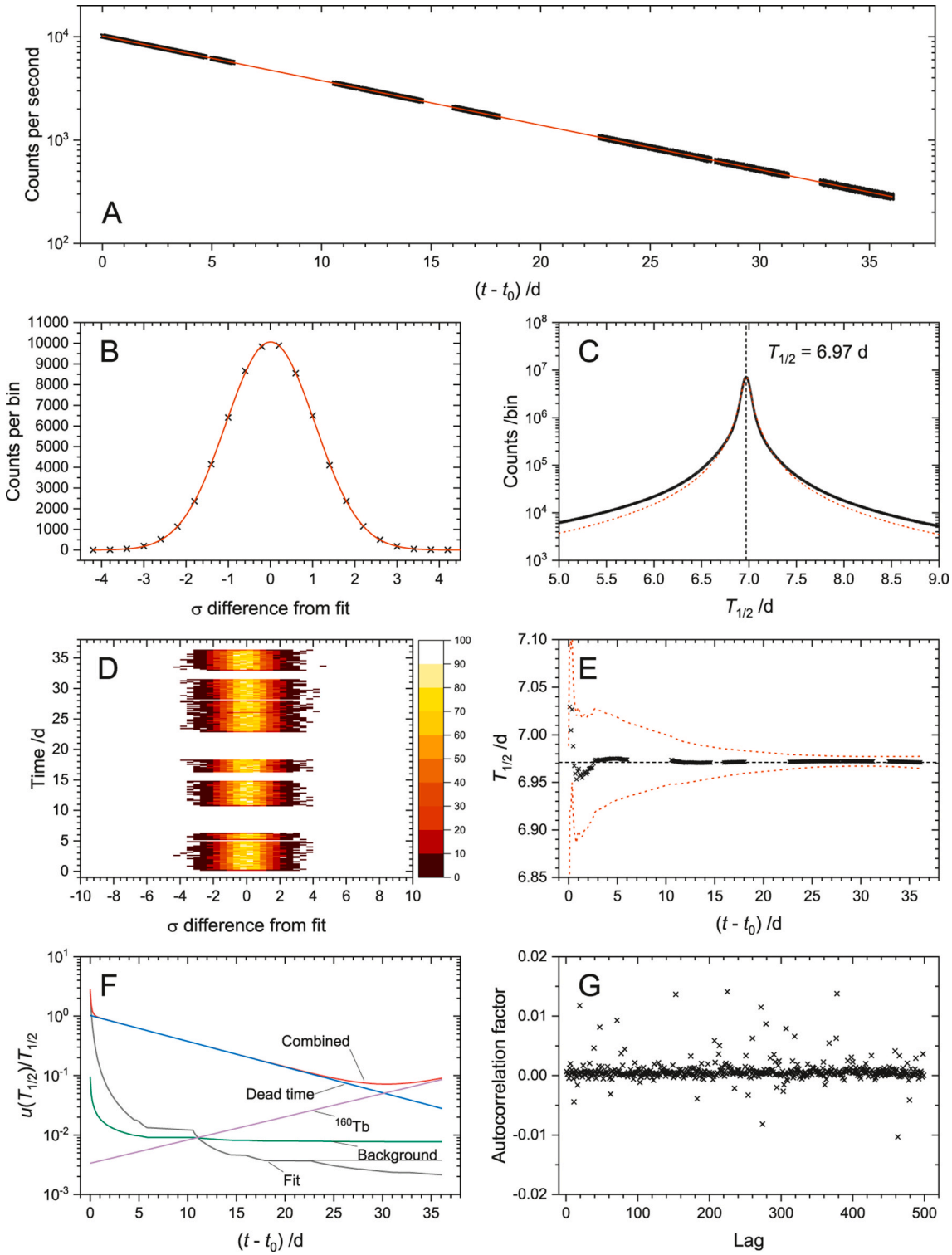

Fig. 13. PNNL half-life evaluation by liquid scintillation counting where (A) depicts the quality of the fit and fit statistics for reference, (B) illustrates the normality of the fit by binning the residuals and fitting with a gaussian, (C) depicts a different method of measuring the half-life obtained by binning the set of all possible half-life estimates using any two points from figure (A), (D) depicts the residual distribution as a function of time, (E) illustrates the stability of the measured half-life and uncertainty over the measurement, (F) is the uncertainty budget as measured over the entire measurement experiment, and (G) is a plot of the autocorrelation of the half-life measurement as a function of lag out to 500 points.

shape due to the delayed and variable charge collection time of the semiconductor relative to the PMTs. These events are believed to be coincidences between gamma events and delayed conversion electrons and after pulses following the beta emission. The clear separation between the background shelf and coincident beta-gamma events was used as a threshold for the beta-coincident gamma spectra; all events between -1400 ns and 2000 ns were defined as true beta-gamma coincidences. Conveniently, this range accounted for more than 99.97% of events in the two PMT distribution (Fig. 11).

Stability of the LSC cocktail was tracked using the ratio of the full-

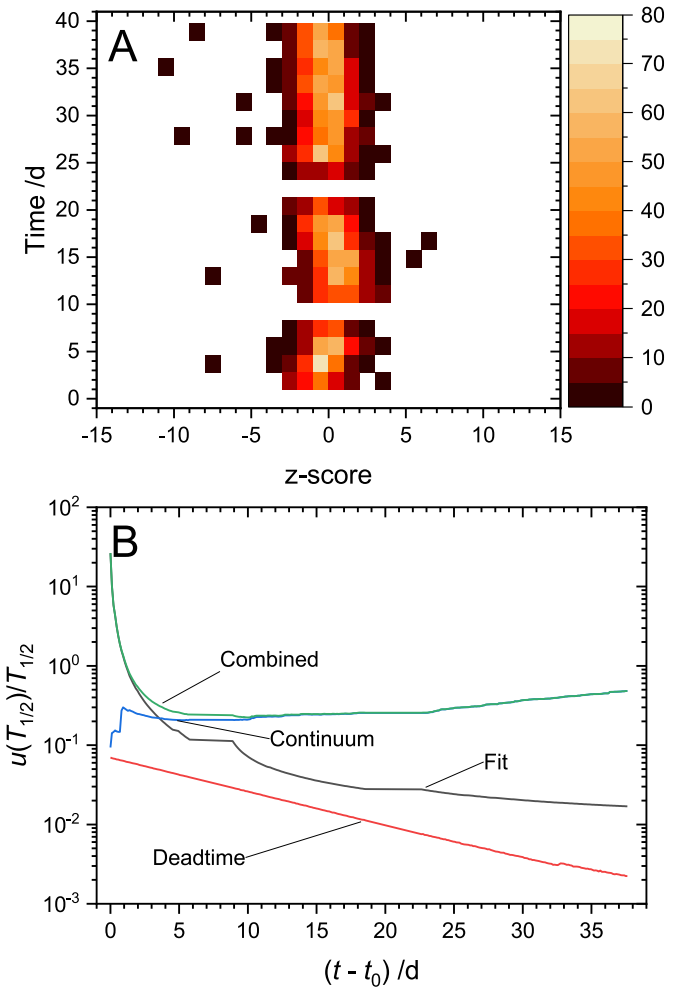

Fig. 14. The (A) Residual distribution and (B) propagated uncertainty with time for the measured half-life using the 74.6 keV gamma-ray emission.

Table 7
Uncertainty budget for the HPGe gamma-ray spectrometry measurements conducted by PNNL. The half-life result is the weighted mean of the three gamma-ray datasets.

Component	25.7 keV		48.9 keV		74.6 keV	
	$T_{1/2}$ /d	$u(T_{1/2})$ /%	$T_{1/2}$ /d	$u(T_{1/2})$ /%	$T_{1/2}$ /d	$u(T_{1/2})$ /%
Statistical		0.015		0.015		0.017
Continuum fitting		0.49		0.55		0.48
Result/energy	6.924 (34)	0.49	6.919 (38)	0.55	6.940 (33)	0.48
Dead time/pile-up		0.0022				
Result	6.929 (20)	0.29				

energy peaks measured freely and in coincidence with the betas over approximately 36 d. Fig. 12 depicts the ratio of gamma rays coincident with beta-emissions (N_C) to the total full-energy peak area (N_γ) for the 25.7 keV, 48.9 keV, and 74.6 keV gamma rays as a function of the count-time. The measured beta detection efficiency ($\varepsilon_\beta = \frac{N_C}{N_\gamma}$) differs for each

Table 8
Summary of half-life measurements made by the different techniques at the three laboratories.

Technique	Laboratory	$T_{1/2}$ /d
Ionisation Chamber	NPL	6.964(15)
HPGe	NPL	6.9588(69)
HPGe	AWE	6.9664(59)
LS	AWE	6.9619(50)
LS	PNNL	6.9710(63)
HPGe	PNNL	6.929(20)
Weighted mean		6.9637(29)
$\chi 2/\nu$		1.04

gamma ray because of differences in the associated beta energy. The maximum observed beta detection efficiency loosely follows this trend; however, the 48.9 keV and 74.6 keV full-energy peaks originate from the same level transition; thus, have an equivalent associated beta continuum. The increase in the measured beta detection efficiency at 48.9 keV is attributed to the additional betas generated by the subsequent conversion of the following level at 25.7 keV. A half-life of 6.9710(63) d was determined by LS counting at PNNL. The uncertainty budget is provided in Table 6. The values of the uncertainty components by both LSC and gamma-ray spectrometry have been estimated through analysis of the data set rather than propagated using Eq. (1).

A rigorous analysis of the LSC data was conducted and is shown in Fig. 13. An exponential curve using Eq. (3) was fit to 30 s count-window integrals corrected for dead-time, stability, and the ^{160}Tb contaminant (Fig. 13a). This half-life estimate was validated by comparing the half-life to an estimate derived from fitting a Lorentzian peak to a histogram of two-point half-life measurements sampled from 66 658 points (Fig. 13c). The normalized residual was also binned and fit using a gaussian to test normality of the data as shown in Fig. 13b. The gaussian width suggests the uncertainty is slightly under-estimated with a standard deviation of 1.13. The residual, forward running half-life, and uncertainty budget as a function of time are also provided in Fig. 13d–f. The uncertainty budget for the final estimate is also provided in Table 6. The dominant source of uncertainty in the case of the measurement by beta was the dead-time with an uncertainty floor at approximately 35 d governed by both dead-time and uncertainty in the ^{160}Tb activity. An evaluation of the autocorrelation is also presented in Fig. 13g.

Measurements of the half-life by gamma-ray spectrometry were nearly an order of magnitude less precise and were more sensitive to sample placement and fitting variations. Fig. 14 depicts the residual as a function of time and depicts the effects of sample placement variation along with the uncertainty budget as measured for the 74.6 keV gamma emission over time. Variations in the continuum produced significant, nearly order percent variations in the peak height of the fitted full-energy peaks. This added variation reduced the precision and consistency of the measured half-life as a function of time; thus, reducing the overall precision with which the half-life could be measured.

Variation in fit affected all three half-life estimates, as shown in Table 7, and served as the limiting factor for precision in the half-life measurement by means of gamma-ray spectrometry at PNNL. The half-life by HPGe gamma-ray spectrometry at PNNL was determined as a weighted mean of the three gamma-ray emissions with a value of 6.929 (20) d.

4. Discussion

4.1. Summary of results

The summary of the results for the six determinations of the half-life of ^{161}Tb, performed by ionisation chamber, liquid scintillation counting and HPGe gamma-ray spectrometry, are presented in Table 8. The results are consistent, with a reduced $\chi 2$ value of 1.04. As three

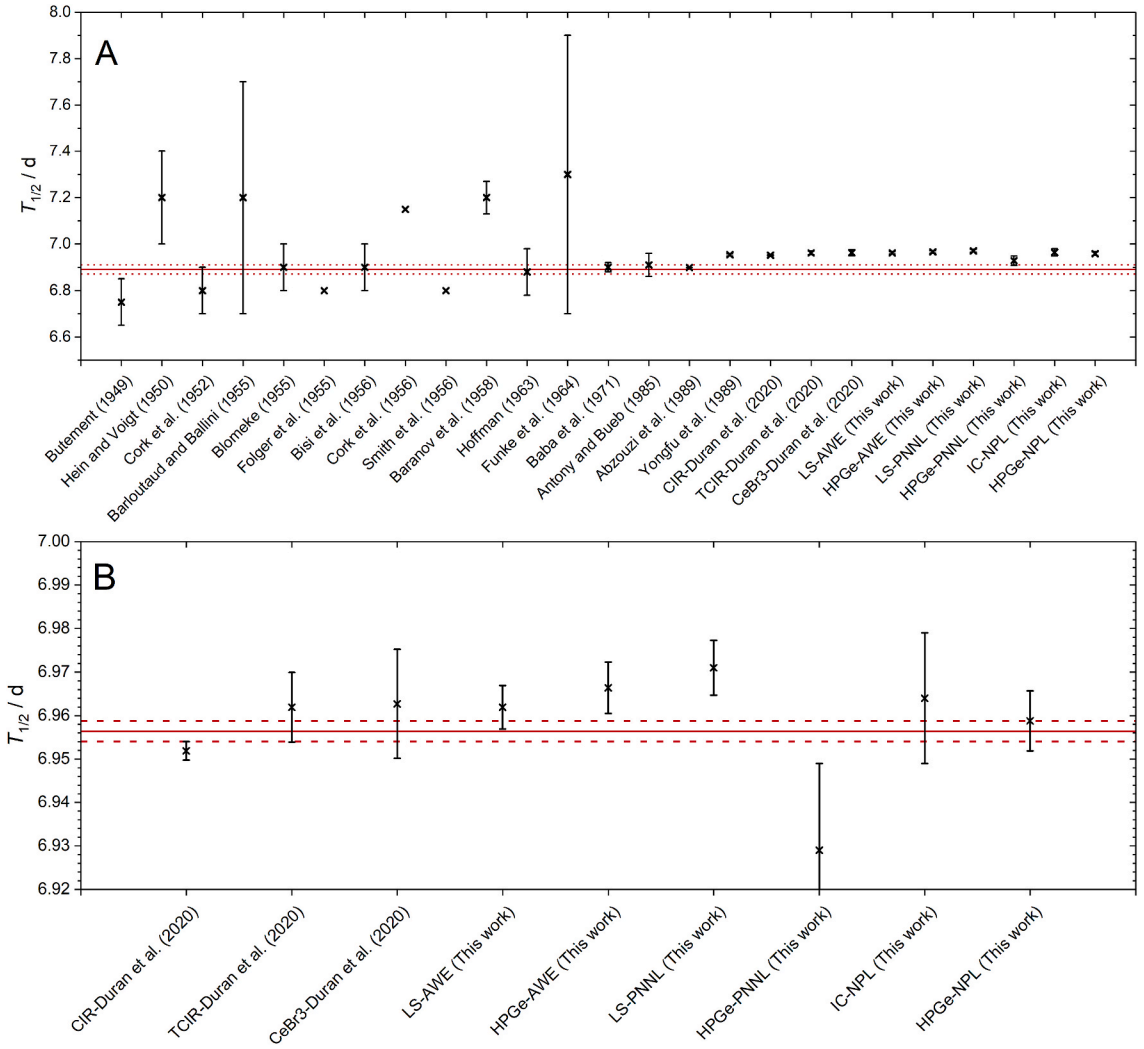

Fig. 15. The half-live values for ^{161}Tb of all literature values are shown in A, with the solid and dashed red lines indicating the evaluated half-and standard uncertainty from Reich (2011). The half-life values determined by Duran at al. (2020) and in this work are shown in B, where the solid and dashed red lines indicate the weighted mean of these half-life values and its standard uncertainty. (For interpretation of the references to colour in this figure legend, the reader is referred to the Web version of this article.)

independent techniques have been used, with uncertainty components that are minimally correlated a weighted mean of the six determinations provides a final $T_{1/2}(^{161}\text{Tb}) = 6.9637(29)$ d.

Typically, it would be expected that the ionisation chamber would provide the most precise result. A consequence of the low initial activity of ^{161}Tb used in this work increased the impact of the background correction and limited the duration of the measurement campaign for the NPL ionisation chamber. Therefore, the precision achieved by the NPL IC is substantially lower than is commonly achievable and of that quoted by Durán et al. (2020) using ionisation chambers. The determinations by the LS and HPGe gamma-ray spectrometry techniques have provided the necessary precision in this work to provide a suitably precise estimate of the half-life.

In the work of Durán et al. (2020) the ^{160}Tb impurity correction for the ionisation chamber relied on the fitting of a^{160}Tb activity parameter in a dual exponential fit. Such modelling of the impurity response in half-life measurements can be prone to significant deviation from the true value due to the impact of noise in the dataset (Bergeron et al., 2021).

Returning to the IC dataset in this work, a dual exponential with a constant background (B) was used, where the pA responses in the IC to ^{160}Tb (I_{160}) and ^{161}Tb (I_{161}), the ^{161} Tb day constant (λ_{161}) and B are free parameters:

$$I(t) = I_{161}(0).e^{-\lambda_1 t}.\frac{1-e^{\lambda_{161}\Delta t}}{\lambda_{161}\Delta t} + I_{160}(0).e^{-\lambda_2 t}.\frac{1-e^{\lambda_{160}\Delta t}}{\lambda_{160}\Delta t} + B \quad (4)$$

From the least-squares fit using Eq. (4) a half-life of 6.9337 d was determined, a relative difference of -0.43% to the half-life reported for the IC when corrected for a known ^{160}Tb response. The values for the I_{160} and B parameters were 0.172 pA and 0 pA respectively. Comparing the ^{160}Tb fit value to the measured value (see section 3.3) this was a significant 22.5% relative increase. This is likely due to the influence of the ^{160}Tb in the total decay curve being small ($pA(^{160}\text{Tb})/pA(^{161}\text{Tb}) =$ 1.6% at the final measurement). It could be expected that a longer measurement campaign would result in a more accurate fit as the ^{160}Tb response is more pronounced in the data. However, this provides a good illustration of size of the errors that could potentially be introduced by a dual exponential least-squares fit where the response of the impurity or background is low and appropriate uncertainties should be estimated as a result. However, it should be noted that the dataset collected in Durán et al. (2020) extends for 23 d and does not have discontinuities due to source repositioning, which may result in a closer approximation of the ^{160}Tb response.

In this work, the response of the ^{160}Tb could be determined due to

the availability of a previously determined calibration factor for IC and through the CIEMAT/NIST efficiency tracing method for LS. The HPGe gamma-ray spectrometers did not require any correction using the full-energy peak areas of the characteristic gamma rays for the decay of ^{161}Tb as these are not interfered by the gamma rays from the decay of ^{160}Tb. This provided confidence in the corrections for the ^{160}Tb impurity and minimised the magnitude of the impact of the ^{160}Tb on the precision of the measurements.

4.2. Comparison against previous literature

The half-lives determined in this work along with previous literature values for the half-life of ^{161}Tb are shown in Fig. 15a in chronological order. The results in the current work, those of Durán et al. (2020) and Yongfu et al. (1989) show a clear and consistent increase of approximately 1% from the half-life evaluated in Reich (2011). As Durán et al. (2020) noted, the previous literature typically lacked information, such as impurity contributions, and did not present a detailed uncertainty budget. Whilst the production route to produce ^{161}Tb in this work and Duran at al. (2020) would always result in some ^{160}Tb present, a lack of correction for this in previous measurements would have resulted in longer half-lives than has been reported which is not the case here.

In Fig. 15b, the half-life results for all measurements reported in this work and Durán et al. (2020) are shown. The weighted mean and its standard uncertainty of the nine measurement results provides a value of $T_{1/2}(^{161}\text{Tb}) = 6.9564(24)$ d with a reduced $\chi^2 = 2.1$, indicating an inconsistent dataset. It can be observed in Fig. 15b that the seven of nine half-life measurements are systematically higher than the weighted mean. Comparing the reported weighted mean of the half-life in both this work and Durán et al. (2020), 6.9637(29) d and 6.953(2) d respectively, they are found to be inconsistent with a ζ-score = 3.1 (ISO, 2015). The quoted precision of the CIR half-life measurement (more than a factor of two more precise than any other reported uncertainty) by Durán et al. (2020) results in a significant weight being attributed to it which leads to a result biased towards that value in both the reported final half-life in their work and in the weighted mean of all nine values in Fig. 15b. The two values reported by Durán et al. (2020) from measurement by the TCIR and the $CeBr_3$ systems, however, are aligned well with those reported in this work.

There is strong evidence from the nine half-life determinations performed between this work and Durán et al. (2020) that the half-life of ^{161}Tb is significantly longer than previously evaluated (ζ-score = 6.5). Further independent measurements, with detailed uncertainty budgets, would be ideal to provide further proof to this observation and to resolve the discrepancy between the half-life reported in this work and that of Durán et al. (2020).

5. Conclusion

The half-life of ^{161}Tb has been determined using the same solution by three independent laboratories in the UK (NPL and AWE) and USA (PNNL). Three independent techniques have been used to observe the radioactive decay of ^{161}Tb: HPGe gamma-ray spectrometry, Ionisation Chamber and Liquid Scintillation Counting. The half-lives determined by the three laboratories using these techniques, for a total of six determinations have been found to be consistent. A half-life of 6.9637(29) d for ^{161}Tb has been determined from the weighted mean of all determinations presented in this work. The half-life determined in this work agrees with the previously determined in Durán et al. (2020) and provides strong evidence that the half-life is significantly higher than previously recommended.

CRediT authorship contribution statement

S.M. Collins: Writing – original draft, Visualization, Validation, Supervision, Software, Methodology, Investigation, Formal analysis, Conceptualization. **C. Gilligan:** Writing – original draft, Methodology, Investigation, Formal analysis, Conceptualization. **B. Pierson:** Writing – original draft, Methodology, Investigation, Formal analysis. **N. Ramirez:** Writing – original draft, Investigation. **M. Goodwin:** Writing – original draft, Investigation, Formal analysis. **A.K. Pearce:** Writing – review & editing, Investigation. **B.C. Archambault:** Writing – review & editing, Formal analysis. **M.M. Haney:** Writing – review & editing, Investigation. **P.H. Regan:** Writing – review & editing, Supervision.

Declaration of competing interest

The authors declare that they have no known competing financial interests or personal relationships that could have appeared to influence the work reported in this paper.

Acknowledgements

The authors wish to thank the Institut Laue-Langevin and the Paul Scherrer Institute for the production and supply of the ^{161}Tb to the NPL. The authors also want to thank Dr Robert Shearman (NPL) for his assistance in the sample preparation. The work performed at NPL was supported in full by the National Measurements System Programmes Unit of the UK's Department for Business, Energy, and Industrial Strategy. C. Gilligan and M. Goodwin acknowledges funding from the UK Ministry of Defence (MoD). P. H. Regan also acknowledges funding from the UK Science and Technologies Facilities Council (grant numbers ST/P005314/1 and ST/001108/1). The work performed at PNNL was funded by the U.S. Department of Defense. Pacific Northwest National Laboratory is operated for the U.S. Department of Energy by Battelle under Contract DE-AC05-76RL01830. The views and opinions of authors expressed herein do not necessarily state or reflect those of the United States Government or any agency thereof.

References

Abzouzi, A., Antony, M.S., Ndocko Ndongué, V.B., 1989. Reevaluation of the half-life of several nuclides. J. Radioanal. Nucl. Chem. 135 (6), 455–460.
Antony, M.S., Bueb, J.B., 1985. Half-life periods of 82Br, 128I, 139Ba and 161Tb. J. Radioanal. Nucl. Chem. 95 (4), 219–225.
Baba, S., Baba, H., Natsume, H., 1971. Half-lives of some fission product nuclides. J. Inorg. Nucl. Chem. 33 (2), 589–595.
Baranov, S.A., Rodionov, Y.F., Shishkin, G.V., Christiakov, L.V., 1958. Energy levels of 161Dy. Soviet Phys. JETP-USSR 5 (6), 946–954.
Barlotaud, R., Ballini, R., 1955. Radioactivité de 159Gd et 161Tb. Comptes rendus hebdomadaires séances Acad. Sci. 241, 389–391.
Bergeron, D.E., Collins, S.M., Pidida, L., Cessna, J.T., Fitzgerald, R., Zimmerman, B., Ivanov, P., Keightley, J.D., Napoli, E., 2021. Ra-224 activity, half-life, and 241 keV gamma ray absolute emission intensity: a NIST-NPL bilateral comparison. Appl. Radiat. Isot. 170, 109572.
Bisi, A., Terrani, S., Zappa, L., 1956. Beta decay of 161Tb and low-lying levels in 161Dy. Nucl. Phys. 1, 425–432.
BSI, 1983. Specification for Ampoules. BS 795. British Standards Institution, London, UK, p. 1983.
Britton, R., Davies, A.V., 2015. Characterisation of a SAGe well detector using GEANT4 and LabSOCS. Nucl. Instrum. Methods Phys. Res. A 786, 12–16.
Brun, R., Rademakers, F., 1997. ROOT — an object oriented data analysis framework. Nucl. Instrum. Methods Phys. Res. Sect. A Accel. Spectrom. Detect. Assoc. Equip. 389, 81–86.
Butement, F.D.S., 1949. Radioactive gadolinium and terbium isotopes. Phys. Rev. 75 (8), 1276.
Collins, S.M., Pearce, A.K., Ferreira, K.M., Fenwick, A.J., Regan, P.H., Keightley, J.D., 2015a. Direct measurement of the half-life of 223Ra. Appl. Radiat. Isot. 99, 46–53.
Collins, S.M., Pommé, S., Jerome, S.M., Ferreira, K.M., Regan, P.H., Pearce, A.K., 2015b. The half-life of 227Th by direct and indirect measurements. Appl. Radiat. Isot. 104, 203–211.
Collins, S.M., Keightley, J.D., Ivanov, P.I., Arinc, A., Fenwick, A.J., Pearce, A.K., 2019. The potential radio-immunotherapeutic α-emitter 227Th - part II: absolute gamma-ray emission intensities from the excited level of 223Ra. Appl. Radiat. Isot. 145, 251–257.
Collins, S.M., Shearman, R., Ivanov, P., Regan, P.H., 2020. The impact of high-energy tailing in high-purity germanium gamma-ray spectrometry on the activity determination of 224Ra using the 241.0 keV emission. Appl. Radiat. Isot. 157, 109021.
Cork, J.M., LeBlanc, J.M., Nester, W.H., Stumpf, F.B., 1952. Energy levels associated with the radioactive decay of 153Gd and 161Tb. Phys. Rev. 88 (3), 685–686.

Cork, J.M., Brice, M.K., Schmid, L.C., Helmer, R.G., 1956. Nuclear levels in 161Dy. Phys. Rev. 104 (2), 481–483.
Durán, M.T., Juget, F., Nedjadi, Y., Bochud, F., Grundler, P.V., Gracheva, N., Müller, C., Talip, Z., van der Meulen, N.P., Bailat, C., 2020. Determination of 161Tb half-life by three measurement methods. Appl. Radiat. Isot. 159, 109085.
Eckerman, K., Endo, A., 2008. Nuclear decay data for Dosimetric calculations. ICRP Publication 107. Ann. ICRP 38, 7–96.
Folger, R.L., Stevenson, P.C., Seaborg, G.T., 1955. High-energy proton spallation-fission of Uranium. Phys. Rev. 98 (1), 107–120.
Funke, L., Graber, H., Kaun, K.H., Sodan, H., Werner, L., 1964. Neue niveaus im 161Dy. Nucl. Phys. 55 (3), 401–409.
Grau, A., Garcia-Toraño, E., 1982. Evaluation of counting efficiency in liquid scintillation counting of pure β ray emitters. Int. J. Appl. Radiat. Isot. 33, 249–253.
Gracheva, N., Müller, C., Talip, Z., Heinitz, S., Köster, U., Zeevaart, J.R., Vögele, A., Schibi, R., van der Meulen, N., 2019. Production and characterization of no-carrier-added 161Tb as an alternative to the clinically-applied 177Lu for radionuclide therapy. EJNMMI Radiopharm. Chem. 4, 12.
Günther, E., 2002. What can we expect from the CIEMAT/NIST method? Appl. Radiat. Isot. 56, 357–360.
Haller, S., Pellegrini, G., Vermeulen, C., van der Meulen, N.P., Köster, U., Bernhardt, P., Schibli, R., Müller, C., 2016. Contribution of Auger/conversion electrons to renal side effects after radionuclide therapy: preclinical comparison of 161Tb-folate and 177Lu-folate. EJNMMI Res. 6, 13.
Hein, R.E., Voigt, A.F., 1950. Radioactive isotopes of gadolinium. Phys. Rev. 79 (5), 783–786.
Hoffman, D.C., 1963. Half-lives of some rare earth nuclides. J. Inorg. Nucl. Chem. 25 (9), 1196–1198.
ISO, 2010. Injection Equipment for Medical Use – Part 1: Ampoules for Injectables. ISO 9187-1:2010. International Organization for Standardization.
ISO, 2011. Control Charts Part 4 Cumulative Sum Charts. ISO 7870-4:2011. International Organization for Standardization.
ISO, 2015. Statistical Methods for Use in Proficiency Testing by Interlaboratory Comparison. ISO 13528:2015. International Organization for Standardization.
Jiang, J., Davies, A.V., Arrigo, L.M., Friese, J.I., Seiner, B., Greenwood, L.R., Finch, Z.S., 2015. Analysis of 161Tb by radiochemical separation and liquid scintillation counting. Appl. Radiat. Isot. 170, 107298.
Jiang, J., Davies, A.V., Britton, R.E., 2017. Measurement of 160Tb and 161Tb in nuclear forensics samples. J. Radioanal. Nucl. Chem. 314, 727–736.
Ku, A., Facca, V.J., Cai, Z., Reilly, R.M., 2019. Auger electrons for cancer therapy – a review. EJNMMI Radiopharm. Chem. 4, 27.
Lehenberger, S., Barkhausen, C., Cohrs, S., Fischer, E., Grünberg, J., Hohn, A., Köster, U., Schibli, R., Türler, A., Zhernosekov, K., 2011. The low-energy β- and electron emitter 161Tb as an alternative to 177Lu for targeted radionuclide therapy. Nucl. Med. Biol. 38, 917–924.
Marin, I., Rydèn, T., Van Essen, M., Svensson, J., Gracheva, N., Köster, U., Zeevaart, J.R., van der Meulen, N.P., Müller, C., Bernhardt, P., 2020. Establishment of a clinical SPECT/CT protocol for imaging of 161Tb. EJNMMI Phys. 7, 45.
Müller, C., Zhernosekov, K., Köster, U., Johnston, K., Dorrer, H., Hohn, A., van der Walt, N.T., Türler, A., Schibi, R., 2012. A unique matched quadruplet of terbium radioisotopes for PET and SPECT and for α- and β^--radionuclide therapy: an in vivo proof-of-concept study with a new receptor-targeted folate derivative. J. Nucl. Med. 53, 1951–1959.
Müller, C., Reber, J., Haller, S., Dorrer, H., Bernhardt, P., Zhernosekov, K., Türler, A., Schibli, R., 2014. Direct in vitro and in vivo comparison of 161Tb and 177Lu using a tumour-targeting folate conjugate. EJNMMI 41, 476–485.
Pommé, S., 2015. The uncertainty of the half-life. Metrologia 52, S51–S65.
Pommé, S., De Hauwere, T., 2020. Derivation of an uncertainty propagation factor for half-life determinations. Appl. Radiat. Isot. 158, 109046.
Reich, C.W., 2005. Nuclear data sheets for A = 160. Nucl. Data Sheets 105 (3), 557–774.
Reich, C.W., 2011. Nuclear data sheets for A = 161. Nucl. Data Sheets 112 (10), 2497–2713.
Sharpe, J., Wade, F., 1951. T.P.A MkII Ionisation Chamber. Report AERE EL/E806. Harwell, Atomic Energy Research Establishment, UK.
Sharpe, J., Wade, F., 1953. A re-entrant thimble ionisation chamber. At.At. Technology 32–33.
Smith, R.R., Reeder, S.D., Lewis, R.H., 1956. Successive neutron capture in 159Tb. J. Chem. Phys. 25 (3), 502–504.
Yongfu, C., Chunguang, Y., Yuzhen, D., 1989. Decay data of 161Tb. In: Behrens, J.W., Carlson, A.D. (Eds.), 50 Years with Nuclear Fission Volume 2. American Nuclear Society, Inc., United States, pp. 949–950.